JOURNAL OF SPACECRAFT AND ROCKETS
Vol. 47, No. 4, July–August 2010

Navier–Stokes Simulations of Hypersonic Flows with Coupled Graphite Ablation

Daniele Bianchi* and Francesco Nasuti†
University of Rome "La Sapienza," 00184 Rome, Italy
and
Emanuele Martelli‡
Second University of Naples, Aversa, 81131 Caserta, Italy

DOI: 10.2514/1.47995

A study of graphite ablation in reentry flows is carried out by a surface ablation approach integrated with a two-dimensional axisymmetric Navier–Stokes solver. The gas–surface interaction model is based on chemical equilibrium ablation with surface mass and energy balances fully coupled with the numerical solver and can account for both surface oxidation and sublimation. The surface temperature is obtained from the steady-state ablation approximation. This numerical procedure can predict aerothermal heating, chemical species concentrations, and carbon material ablation rate over the heat-shield surface of reentry vehicles. Two-dimensional axisymmetric simulations have been performed to numerically reproduce the ablation of a graphite sphere cone that has been tested in the Interaction Heating Facility at the NASA Ames Research Center. The freestream conditions of the selected test case are typical for Earth reentry from a planetary mission. The predicted ablation rate and surface temperature assuming frozen chemistry in the flow show a good agreement with the available experimental data. The agreement is further improved freezing the nitrogen recombination reaction at the surface to be more consistent with experimental observation, which has shown nitrogen atom recombination not to occur at the graphite surface.

Nomenclature

A	=	cross section area, m^2
D_{im}	=	effective diffusion coefficient, m^2/s
h	=	enthalpy, J/kg
k	=	thermal conductivity, $W/m \cdot K$
$\dot{m}$	=	mass blowing rate per unit area, $kg/m^2 \cdot s$
N_c	=	number of species
N_{el}	=	number of elements
p	=	pressure, N/m^2
$\dot{q}$	=	heat flux per unit area, W/m^2
r	=	distance from surface, m
$\dot{s}$	=	recession rate, m/s
T	=	temperature, K
t	=	time, s
u	=	streamwise velocity, m/s
v	=	velocity component normal to surface, m/s
W	=	molecular weight, kg/k mole
Y	=	elemental mass fraction
y	=	species mass fraction
y^+	=	dimensionless wall distance
α_{ki}	=	mass fraction of element k in species i
ΔH_{abl}	=	heat of ablation, J/kg
ϵ	=	surface emissivity
η	=	outward coordinate normal to surface
ρ	=	density, kg/m^3
σ	=	Stefan–Boltzmann constant

Subscripts

i	=	species
k	=	element
s	=	solid (graphite) properties at gas–solid interface
s_i	=	solid (graphite) properties at initial conditions
w	=	gas properties at gas–solid interface

Received 4 November 2009; revision received 28 April 2010; accepted for publication 6 May 2010.

*Research Fellow, Department of Mechanics and Aeronautics, via Eudossiana 18. Student Member AIAA.

†Associate Professor, Department of Mechanics and Aeronautics, via Eudossiana 18. Senior Member AIAA.

‡Assistant Professor, Department of Aerospace and Mechanical Engineering, via Roma 29. Student Member AIAA.

I. Introduction

UPON exposure to ballistic reentry environments, ablative thermal protection systems (TPS) are subjected to severe thermal and mechanical conditions and must be designed to keep the excessive heat from damaging the vehicle with a minimum weight penalty. In highly energetic hypersonic environments, TPS materials interact with the flow through diverse thermochemical and thermophysical mechanisms including ablation, spallation, and solid thermal conduction. Surface chemical reactions play a significant, if not dominant, role in establishing the ablation mass flow and energy transfer rate at the heated surface. The boundary layer heats up the surface, due to convection and radiation from the hot gases. Moreover, due to the presence of chemical reactions at the wall, there are gradients of concentrations inside the boundary layer. The heat flux toward the surface is partly convected inside the material and partly reradiated from the hot surface, which can reach temperatures over 3000 K. The chemical reactions between the TPS and the boundary layer generate gaseous products that are injected in the boundary layer, reducing the convective heat flux to the wall (blockage effect). The correct understanding and accurate modeling and simulation of the gas–surface interaction phenomena have a key role in the design of the ablative TPS. In recent years, computational fluid dynamics (CFD) technology has continued to develop in the areas of nonequilibrium flow, multispecies kinetics, and multi-dimensional full Navier–Stokes capabilities. However, most codes use standard surface boundary conditions and cannot be realistically used to predict the aerothermal heating for the design of TPS [1]. In fact, CFD codes typically treat fluid/solid boundary conditions in a very simplified manner, such as constant prescribed temperature or heat flux and zero mass transfer. Current methods focus their attention on some aspects of the problem at the expense of others [2,3]. Thus, aerodynamic methods concentrate on the flowfield and

rely on other methods to provide material-response characteristics; on the other hand, material-response methods concentrate on surface ablation and heat conduction in the material, using simplified models and correlations to provide the aerothermodynamic heating. However, in reality, all these phenomena are highly coupled. To obtain a suitable tool for the analysis of flowfield with ablation, CFD codes must take into account spatially varying surface temperature and heat flux, a realistic surface energy and multispecies mass balances, thermal soak into the TPS material, and thermochemical ablation modeling.

The objective of this study is to extend to the case of reentry flows the validation of the full Navier–Stokes approach coupled with a thermochemical equilibrium ablation model presented in [4]. The importance of a coupled analysis for ablating flowfield predictions has been assessed in [5] and recently confirmed by the analysis made by Johnston et al. [6], who have shown the inaccuracies due to the approximations typically used for uncoupled and partially coupled ablation-flowfield analyses in several ablation cases. Yet the Navier–Stokes approach used in [6] is different from the present one because of the numerical scheme adopted, the numerical treatment of the ablation boundary conditions, the ablation regime, and the surface material. The attention of the present study is focused on both diffusion-limited oxidation and sublimation for graphite heat shields. Thermomechanical ablation or spallation is neglected in this work, because many researchers [7–9] have concluded that the thermochemical ablation of graphite is the primary reason for the TPS ablation. Validation is carried out by comparison of computed results with literature data on the ablation of a graphite sphere-cone model [9,10].

II. Theoretical Modeling

In the present formulation the gas-phase dynamics is based on the full Navier–Stokes equations for single-phase multicomponent reacting systems in which variable thermodynamic and transport properties are accounted for. The heat conduction process in the solid material is treated as being one-dimensional and steady-state. An accurate evaluation of the boundary-layer mass and energy transfer mechanism is a key issue to predict the correct mass blowing rate, wall temperature, and consequently the heat flux over an ablating surface. Simplified approaches based on boundary-layer transfer-coefficients require less CFD code modifications but rely on a less accurate modeling, which can limit the accuracy in the estimation of surface ablation rate and heat flux. To obtain a better evaluation of the ablating flowfield, the mass and energy exchange mechanisms must be accurately modeled using the information from the Navier–Stokes solver; this has been performed integrating the numerical solver with a computational surface thermochemistry technique.

A. Governing Equations for the Gas Phase

To study the complex flowfield over an ablating surface, a Navier–Stokes approach has been used in this work taking into account heterogeneous chemical reactions at the surface, rate of diffusion of the species through the boundary layer, heat conduction inside the material, and variable multispecies thermophysical properties. The physics of the hot gases over a solid surface is modeled by the chemically reacting Navier–Stokes governing equations written for 2-D axisymmetric flows.

B. Governing Equations for the Solid Phase

The heat conduction in the solid material is an important mechanism that has to be considered in the recession analysis. However, when a coupling with a material-response code is not available, further hypothesis have to be made in order to compute the solid conduction term [1]. It is assumed that heat conduction into the material is dominant in the direction normal to the surface. In a moving local coordinate system tied to the receding surface, the temperature distribution at a given distance y from the surface is governed by the following equation [11]:

$$\rho_s \frac{\partial h_s}{\partial t} = \frac{1}{A}\frac{\partial}{\partial y}\left(k_s A \frac{\partial T_s}{\partial y}\right) + \rho_s \dot{s}\frac{\partial h_s}{\partial y} \tag{1}$$

The terms in Eq. (1) represent, from left to right, the sensible energy accumulation, the net conduction, and the net energy convected as a consequence of coordinate motion. A closed-form solution of the heat conduction equation at steady state [5,12] is available integrating Eq. (1) between the solid–gas interface and the body inner wall assuming adiabatic condition for the latter, constant cross section area and steady-state condition leading to $\dot{q}_s = -k_s \partial T_s/\partial r = \dot{m}(h_s - h_{s_i})$. This approximation is made in the present study, because the heating of the material in reentry environment is generally very quick [13]; the surface temperature rises rapidly during the first few seconds of exposure and then increases very slowly with time, denoting an almost steady-state condition [14–16]. A radiative equilibrium solution could be achieved by neglecting the solid conduction term, however, this is rarely a reasonable assumption. The steady-state ablation is a much better assumption than the radiative equilibrium, because the conduction heat flux is, in general, larger than the steady-state value and tends to it asymptotically with time (provided that the external conditions are not varying).

C. Gas–Surface Interactions

Because of the chemically active surface, further physical modeling is necessary for the gas–surface interaction. A method based on surface chemical equilibrium has been developed to examine thermochemical ablation of protection materials, which includes all the relevant physics of the complex interaction between a hot-gas layer and the graphite TPS. The two regions, gas and solid, are fully coupled at the surface by appropriate energy and mass balances. This allows the surface conditions to be solved as part of the overall solution. CFD solutions are hence computed taking into account surface blowing and solid conduction. Consider the fluxes of mass entering and leaving a control surface fixed to the ablating surface. If it is assumed that no material is being removed in a condensed phase, due to mechanical erosion (spallation) and neglecting the gas radiation, then the surface mass and energy balances (Figs. 1 and 2) for a noncharring ablating surface can be written as

$$\rho D_{im}\left.\frac{\partial y_i}{\partial \eta}\right|_w + \dot{m}_i = (\rho v)_w y_{i_w} \qquad i = 1, N_c \tag{2}$$

which is the surface mass balance, and

$$k\left.\frac{\partial T}{\partial \eta}\right|_w + \sum_i^{N_c} h_{i_w}\rho D_{im}\left.\frac{\partial y_i}{\partial \eta}\right|_w + \dot{m}h_s = (\rho v)_w h_w + \epsilon\sigma T^4 + \dot{q}_s \tag{3}$$

which is the surface energy balance.

The terms on the left-hand side of Eq. (2) are the mass fluxes of species i entering the surface, due to diffusion and heterogeneous surface reactions, respectively, and the term on the right-hand side is the mass flux of species i leaving the surface, due to surface ablation (blowing). The source term $\dot{m}_i$ is positive for the ablation products and negative for the oxidizing species that are consumed in the ablation process.

The terms on the left-hand side of Eq. (3) are the heat fluxes entering the surface, due to conduction from gas, diffusion, and surface motion, respectively, and the terms of the right-hand side are

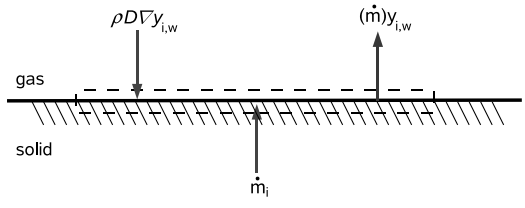

Fig. 1 Surface mass balance.

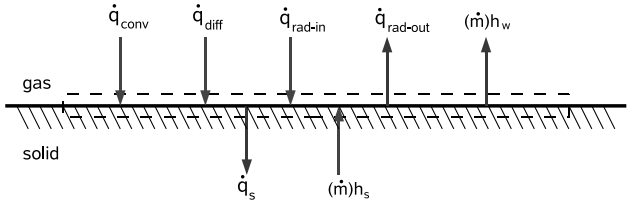

Fig. 2 Surface energy balance.

the heat fluxes leaving the surface, due to surface ablation, reradiation from surface, and conduction in the material. The conduction term $\dot{q}_s = -k_s \partial T_s / \partial r$ is represented by a closed expression available at steady state from Eq. (1). Thus, the solid- and gas-phase boundaries are coupled at the interface.

A summation of Eq. (2) over all the species yields the total mass rate:

$$\sum_i \dot{m}_i = (\rho v)_w = \dot{m} \tag{4}$$

Now introducing in Eq. (2) the variable $y_{i_s} = \dot{m}_i / \dot{m}$, which is the mass fraction of species i produced or consumed in the ablation process per mass of TPS material ablated, and substituting Eq. (2) into Eq. (3), yields a compact form of the surface energy balance:

$$k \left.\frac{\partial T}{\partial \eta}\right|_w - \dot{m} \Delta H_{\text{abl}} = \epsilon \sigma T^4 + \dot{q}_s \tag{5}$$

The term

$$\Delta H_{\text{abl}} = \left(\sum_i h_{i_w} y_{i_s} - h_s \right)$$

is the heat of ablation, which is the difference between the enthalpies of the species created or consumed by the ablation process and the enthalpy of the solid material at the surface temperature per mass of material removed; hence the term $-\dot{m} \Delta H_{\text{abl}}$ represents the heat flux absorbed (when negative) by the thermochemical ablation process that will be referred to as *chemical heat flux*.

Heterogeneous reactions consume the oxidizing species at the surface and thereby create species concentration gradients in the boundary layer, which result in the diffusion of oxidizing species to the surface. Thus, the ablation rate will depend on both the diffusion rate of oxidizing species across the boundary layer to the wall and on the chemical kinetic rates of heterogeneous reactions at the surface: the lowest rate process will control the rate of the overall ablation process. If the surface temperature is sufficiently high, the chemical reactions become sufficiently fast to consume all the oxidizing species diffusing to the surface and local chemical equilibrium is established at the solid–gas interface. When such a condition is reached, the ablation process is considered diffusion-limited and the solution is not dependent on the kinetic rates of the heterogeneous surface reactions. The equilibrium assumption is considered as an acceptable approximation when surface temperature exceeds 2500 K for the application of interests. Usually such a temperature is easily reached in high-speed reentry applications in which ablative TPS are employed. The surface equilibrium approach provides satisfactory accuracy with reduced computational cost, although a full non-equilibrium model is required for the most general case. However, little data are available to validate gas–surface kinetic models that strongly affect the prediction of mass blowing rate. Zhluktov and Abe [16] noted that even if a vast literature exists on the carbon surface chemistry, there is no common opinion among investigators about the main processes on the carbon surface, and Havstad and Ferencz [7] confirmed that despite the maturity of the field, models for the surface chemical kinetics differ from study to study. On the contrary, to calculate the equilibrium state of a chemical system, information relative to all chemical reactions is not needed, and a significant simplification in the problem formulation is obtained. Because of this significant simplification and its validity in most of the applications of interest, the surface equilibrium assumption is made in the present study.

Within the assumption of surface equilibrium it is convenient to express the surface mass balance in terms of the elemental mass fractions Y_k, which are known for the TPS material and which are unknown at the gas–surface interface. A weighted summation of Eq. (2) over all the species yields a balance equation for each element k:

$$\sum_i \alpha_{ki} \rho D_{im} \left.\frac{\partial y_i}{\partial \eta}\right|_w + \dot{m} Y_{k_s} = \dot{m} Y_{k_w} \qquad k = 1, N_{\text{el}} \tag{6}$$

The term $Y_{k_s} = \dot{m}_k / \dot{m}$ is the mass fraction of element k produced in the ablation process per mass of TPS material ablated and must be equal to the elemental composition of the TPS material. The use of Eq. (6) together with the assumption of chemical equilibrium at the wall permits bypassing the entire discussion about the reaction mechanisms and the associated reaction rates, especially for the complex flowfields with ablation. The surface equilibrium approach provides, in most cases, satisfactory accuracy with reduced computational cost and can account for both oxidation and sublimation of carbon. Figure 3 shows the equilibrium chemical composition for carbon ablation in air at different pressures obtained using a free-energy minimization procedure [17]. The surface composition can be evaluated for temperatures below the sublimation temperature (which depends on pressure), above which graphite is not present in solid phase. The major sublimation product is the species C_3, with C_5 playing an important role only at high pressures and temperatures.

The other boundary conditions at the solid–gas interface are

$$u = 0, \qquad v = \dot{m}/\rho, \qquad \partial p / \partial \eta|_w = 0 \tag{7}$$

Solving the surface energy and mass balances (5) and (6) permits evaluating the ablation mass rate and the surface temperature.

III. Numerical Procedure

The analysis of the reentry flowfield is performed by a 2-D axisymmetric time-accurate multispecies Reynolds-averaged Navier–Stokes solver [18–20]. The equations are numerically solved following the *lambda scheme* [20] using a curvilinear orthogonal frame, in order to have a grid well adapted to the geometry of the body, which is transformed to a Cartesian grid by conformal mapping. The technique is second-order-accurate and its simplicity yields a reduction of computational time compared to other techniques. Moreover, it permits easy handling of boundary points and boundary conditions. This simplicity and accuracy in treating the boundaries is especially useful for the treatment of complex boundary conditions, as in the case of ablation. The thermodynamic properties for individual species are approximated by seventh-order polynomials of temperature and the transport properties are approximated by fourth-order polynomials [17]. Mixture properties for conductivity and viscosity are derived from Wilke's rule. The diffusion model is based on an effective diffusion coefficient obtained assuming a constant Lewis number. All computations are made considering graphite as surface material, whose thermodynamic properties as a function of temperature are taken from literature data [17]. Assuming surface equilibrium, the chemical composition at the surface (y_{i_w}) can be obtained using a free-energy minimization procedure [17]. The ablation mass rate is then computed from the elemental mass balance equation (6) and the known surface chemical composition. The surface temperature is computed from the surface energy balance equation (5) using the Newton's iterative procedure. At each computational iteration, the surface temperature, the mass blowing rate, and the wall chemical composition are continuously updated until a steady-state condition is reached.

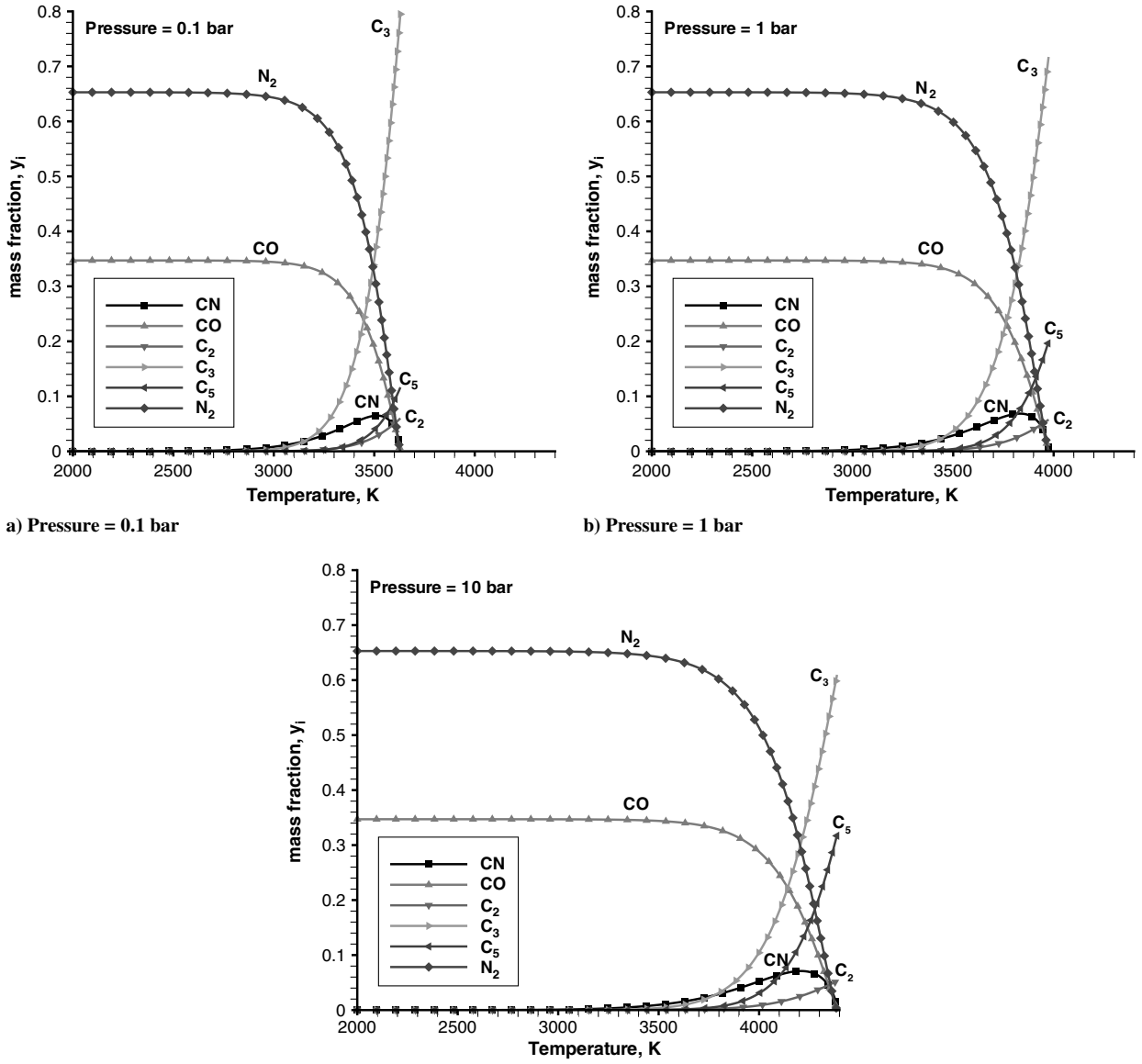

a) Pressure = 0.1 bar

b) Pressure = 1 bar

c) Pressure = 10 bar

Fig. 3 Equilibrium chemical composition for carbon ablation in air at different pressures.

IV. Results and Discussion

The model described in the preceding sections is implemented to simulate the heat-shield ablation in practical reentry environments. The graphite model is a 10 deg half-angle sphere cone with nose radius of 1.905 cm and a total length of 8.89 cm, which has been tested in the Interaction Heating Facility at the NASA Ames Research Center (ARC) [9,10].

Two-dimensional axisymmetric simulations have been performed to numerically reproduce this test case. The computational domain is subdivided into two zones: one for the spherical region and one for the conical region with 40×60 and 60×60 grid points in the axial and normal directions, respectively. In the normal direction, meshes are clustered near the body surface such to accurately capture the near wall phenomena. All the computations presented are at steady-state condition and a grid sensitivity analysis has been carried out to ensure that results are grid independent. The blunted cone is exposed to a laminar supersonic flow of dissociated air coming from the arc jet. The flow conditions, which are those corresponding to the experimental test [10], are listed in Table 1. In this arc stream, oxygen is fully dissociated and nitrogen is partially dissociated. The ablation species considered are CO (oxidation) and C_3 (sublimation) and the flow species are those listed in Table 1. The overall number of species included in the gas is therefore 6: specifically, N_2, NO, N, O, CO, and C_3. Recently, the importance of argon injection in the ARC arc jets has been recognized and reported [21]. As the argon fraction is increased, the oxygen fraction is decreased, thus reducing the surface recession due to oxidation. The relative magnitude of this decrease has been reported only for the phenolic impregnated carbon ablator material in the sole oxidation regime and it is shown to reduce for increasing heat fluxes. The highest heat flux considered in [21] is 970 W/cm^2 and the corresponding stagnation-point recession shows a little effect of oxygen dilution by argon. The test case

Table 1 Freestream conditions for the test case

Property	Value
Velocity	5354 m/s
Density	0.003 kg/m^3
Temperature	1428 K
Mass fractions	
C_{O_2}	0.0
C_{N_2}	0.6169
C_{NO}	0.0046
C_N	0.1212
C_O	0.2573

considered here (whose argon mass fraction has not been found in the open literature) is much more severe with a cold wall heat flux of 2100 W/cm^2, which causes major sublimation in the stagnation region. For that reason, it is deemed not necessary to include argon mass fraction in the computation. Flowfield pressure contours are reported in Fig. 4 showing the bow shock ahead of the body. The predicted stagnation-point pressure is 0.79 atm in accordance with the experimental data of 0.80 atm reported in [10]. The maximum computed fluid temperature behind the shock is above 10,000 K, as predicted in [9]. In the present simulations, the flowfield is assumed frozen, and chemical reactions are considered only at the ablating surface, to focus the attention on the heterogeneous surface reactions. Once the wall composition has been calculated, the species are not allowed to react with each other, as they are diffusing across the boundary layer. The flowfield frozen-chemistry assumption is reasonable for simulated high-energy hypersonic flows, in which the high-speed gas is already dissociated, due to the arc heating and flowfield nonequilibrium effects are of minor importance [22]. Figure 5 shows the predicted carbon mass blowing rate and surface temperature distributions along the graphite surface together with the experimental data measured. Both mass blowing rate and temperature are maximum at the stagnation point, where there is maximum heat flux. Surface temperature prediction is compared with the experimental temperature distribution measured using an infrared camera and pyrometers at the ARC arc-jet facility.

The present model slightly overpredicts the surface temperature: from 3 to 5% in the spherical region and from 6 to 30% in the conical region. The results are very satisfying, especially when considering that the surface chemical equilibrium assumption is acceptable for surface temperatures above 2500 K. Therefore, when temperature drops below this value results can be affected by a certain degree of inaccuracy. The two dots at the stagnation point and at 45 deg from the stagnation point represent the measured mean graphite mass blowing rates after the 30 s heat pulse. Around the nose-tip region the predicted mass blowing rate is ~25% higher than the measured rate. The difference between the prediction and the experimental data at 45 deg from the stagnation point is less than 5%. Note that the finite rate ablation models used in [10] showed an error on the predicted mass blowing rate of ~25% at the stagnation point and of ~20% at 45 deg from the stagnation point. It has to be reminded that surface recession, which is a strong function of the heating rate, tends to blunt the spherical nose, and thus reduce stagnation-point heating. The coupled CFD/Thermal analyses presented in [9] show that the shape change effect is not strong for the selected sample problem and it affects the solution only in the stagnation point, where the heat flux at the end of the heat pulse is 90% of that at the beginning. Such a variation is a second-order effect, which has not been considered predominant in the present work and hence has not been accounted for to avoid fully coupled flow/solid simulation and to focus on the study of surface ablation in the oxidation and sublimation regime. Figure 6 shows the CO mass fraction at the surface and the CO production term [$\dot{m}_{CO}$ according to Eq. (2)], which is the result of the surface heterogeneous reactions among graphite and the oxidizing species present in the flowfield. Carbon monoxide mass fraction at the surface is increasing from the spherical to the conical region showing that graphite oxidation becomes dominant in the conical region of the body. The surface CO production is decreasing along the surface, however, due to the reducing ablation rate (see Fig. 5). Figure 7 shows the CO mass fraction profiles inside the boundary layer at different positions along the surface; CO is produced at the surface, due to heterogeneous reactions and is diffusing from the surface to the boundary layer. Figures 8 and 9 show the same results for species C_3. Graphite sublimation (detected by C_3 formation) is dominant in the spherical region and is absent in the conical region. The transition between sublimation and oxidation of graphite is clearly shown in Figs. 6 and 8. The mass fraction of CO along the wall is increasing and reaches its maximum in the conical region of the blunt body. The mass fraction of C_3, instead, is maximum at the stagnation point, where the surface temperature reaches its highest value and then decreases up to zero at the beginning of the conical region, due to a too-low surface temperature. The C_3 production term is positive in the stagnation-point region and then becomes negative

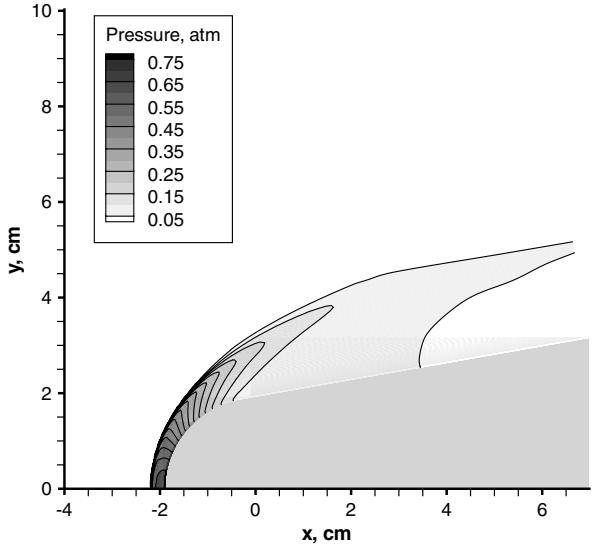

Fig. 4 Flowfield pressure contours.

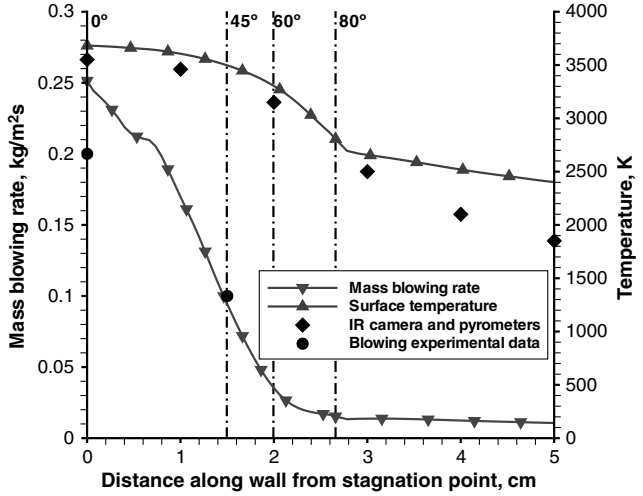

Fig. 5 Predicted surface temperature and mass blowing rate distributions along the surface (IR denotes infrared).

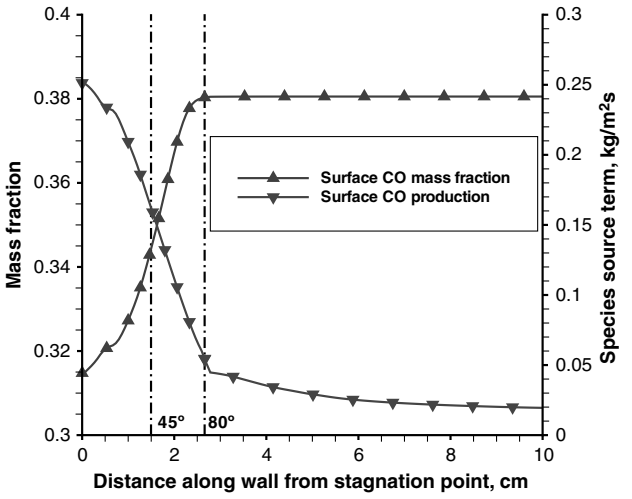

Fig. 6 Predicted CO mass fraction and CO production distribution along the surface.

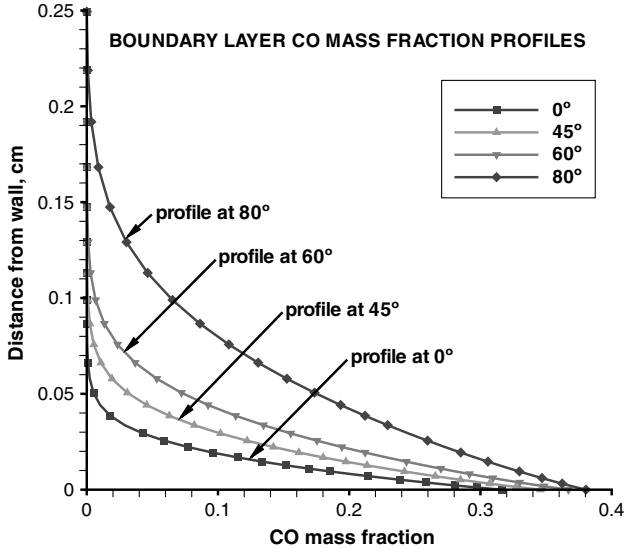

Fig. 7 Predicted CO mass fraction profiles at different positions along the surface.

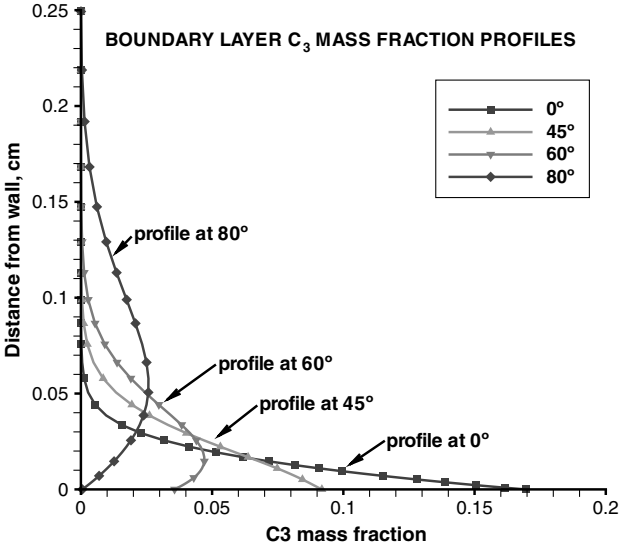

Fig. 9 Predicted C3 mass fraction profiles at different positions along the surface.

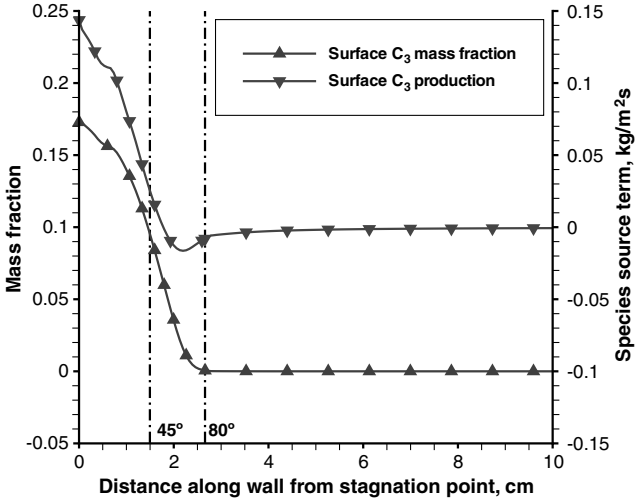

Fig. 8 Predicted C3 mass fraction and C3 production distribution along the surface.

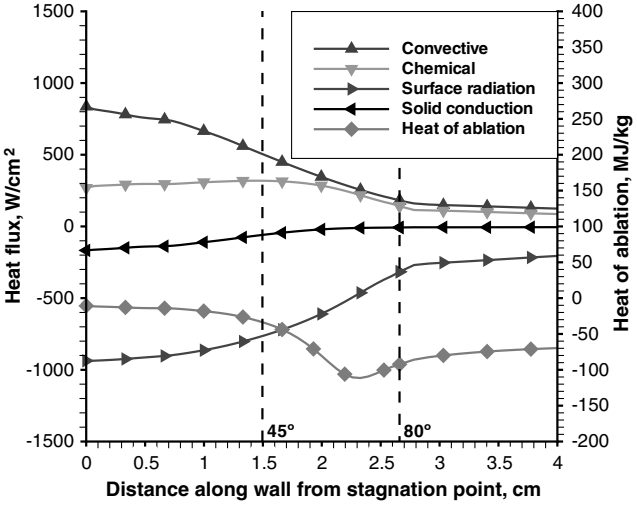

Fig. 10 Predicted heat flux distributions along the surface.

after 45 deg, denoting a consumption (recondensation) of gaseous C_3 at the solid surface, due to the lower surface temperature at this position. Looking at Fig. 9, it is interesting to observe that upstream of the 45 deg point, the C_3 profiles show a maximum at the surface, whereas downstream of the 45 deg point they show a maximum away from the surface; this is due to the fact that the C_3 mass fraction at the wall is decreasing along the surface, whereas the higher amount of C_3 produced in the stagnation-point region is being convected downstream. After 45 deg from stagnation point, gaseous C_3 is diffusing toward the surface. The wall heat flux distributions along the surface are presented in Fig. 10. The sum of the various terms is zero according to the surface energy balance equation (5). The stagnation-point convective heat flux of 800 W/cm^2 is very close to the prediction of Chen and Milos [10] with the Zhluktov finite rate model. Nearly 25% of the incoming convective heat flux is conducted inside the material at the stagnation point, thus showing the inaccuracy of a radiative equilibrium assumption for such a case. Moreover, the surface reradiation, due to the high wall temperature, plays a major role in cooling the stagnation point. The chemical heat flux due to heterogeneous surface reactions is positive (entering the surface) according to the fact that the chemical reactions at the surface are releasing heat (carbon oxidation in air is highly exothermic). Although carbon sublimation is an endothermic process, the heat release due to carbon oxidation is higher than the heat absorbed by the sublimation process. However, due to sublimation, the chemical heat flux is not maximum at the stagnation point, as occurs for the other heat fluxes, but reaches its highest value at 45 deg from stagnation point. This behavior can be better understood by looking at the heat of ablation in Fig. 10, which is highest (but still negative) at the stagnation point, where sublimation is maximum. Figure 11 shows the difference in the convective heat flux with and without the effect of ablation products injection (blowing); the solution without blowing has been computed assigning the same surface temperature profile of the solution with blowing. The solution without blowing shows a convective heat flux, which is 20% higher (at the stagnation point) than the one with blowing. This difference is the so-called blockage effect, i.e., a reduction of the heat flux, due to the blowing effect. The blockage effect is maximum at the stagnation point and goes to zero in the conical region, where there is little to no blowing.

Figure 12 presents the chemical species distributions along the stagnation streamline. The results indicate that CO and C_3 are both produced at the surface, whereas O, NO, and N are completely consumed in the ablation process. Molecular oxygen is not represented, because its mass fraction is zero in the freestream conditions. Chemical equilibrium calculations at the stagnation point predict both graphite oxidation and sublimation together with atomic

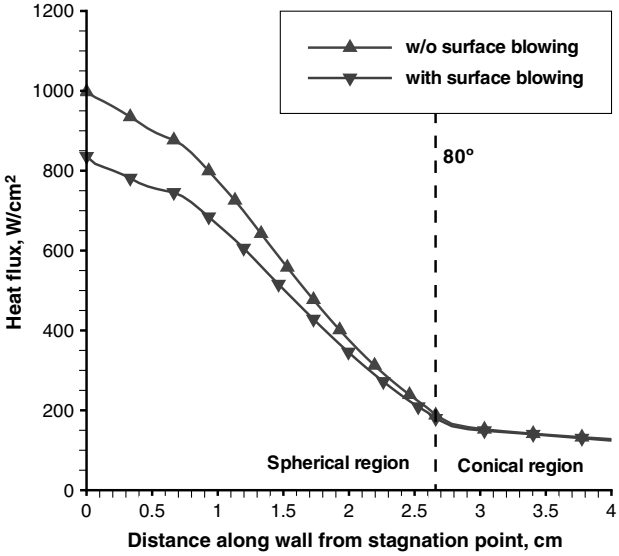

Fig. 11 Predicted convective heat flux distributions with and w/o surface blowing.

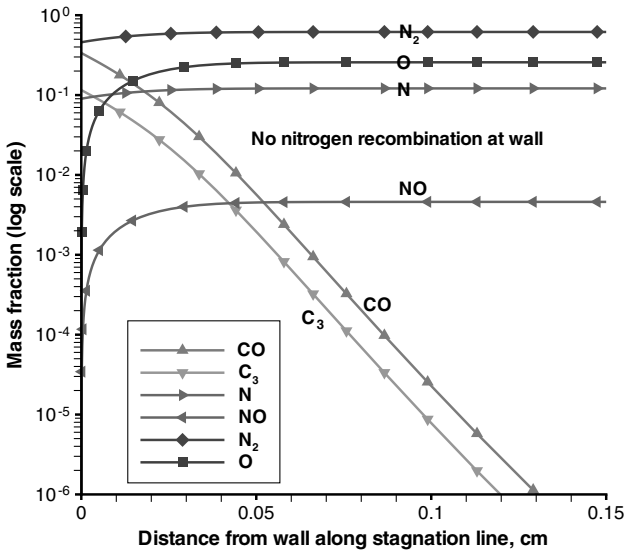

Fig. 13 Chemical species distributions along the stagnation streamline without atomic nitrogen recombination.

nitrogen recombination. At the actual surface pressure and temperature conditions, in fact, the surface equilibrium computation predicts a complete recombination of N to N_2. However, as shown by Park [23,24], the surface catalysis reactions are shown to be negligibly small for both oxygen atom and nitrogen atom recombination at the graphite surface. According to surface equilibrium, oxygen recombination is not an issue, because all the free oxygen (atomic or molecular) reacts completely to form carbon monoxide at the surface. The atomic nitrogen present in the flow, instead, is completely consumed at the surface, as Fig. 12 clearly shows. Since the surface catalytic nitrogen recombination has never been seen experimentally at the graphite surface [24], the present test case has been recomputed freezing this recombination reaction. The ratio between N_2 and N at the surface is kept frozen to its edge value, thus not allowing the nitrogen recombination to happen; this treatment is useful for species that are relatively nonreacting because of chemical kinetic effects. Note that the edge ratio between N_2 and N is constant and equal to the freestream value, since the flowfield is assumed frozen. Figure 13 shows the chemical species distributions along the stagnation streamline without atomic nitrogen recombination at the wall. The mass fractions of N and N_2 along the stagnation streamline is slightly decreasing, due to the blowing effect, but their ratio is not changing. The effect of nitrogen recombination inhibition on both surface temperature and ablation rate is shown in Figs. 14 and 15. The pressure distribution along the surface is in excellent agreement with the one presented in [10] and remains completely unaffected by this change in surface composition, whereas the surface temperature is reduced and the agreement with the experimental data is improved. An even stronger effect can be seen on the ablation rate, which is noticeably reduced, especially in the proximity of the stagnation point, where the gradients are higher and hence more nitrogen is diffused toward the surface. The lack of heat release by the nitrogen recombination reaction produces a decrease in surface temperature, which in turn decreases the material sublimation and consequently the ablation rate. The predicted mass blowing rate is only 1.5% higher than the measured rate at the stagnation point and about 23% lower at 45 deg from the stagnation point with the frozen atomic nitrogen concentration. Thus, the model prediction improves noticeably in the stagnation point, whereas it gets worse at the 45 deg location. The effect of nitrogen recombination inhibition on ablation species production is finally shown in Fig. 16; the sublimation of carbon in the stagnation point is reduced by the lower surface temperature, whereas the carbon oxidation is consequently increased. These results show the strong coupling between the surface temperature and the surface mass blowing rate in the sublimation regime: a slight reduction (2%) of the surface temperature at the

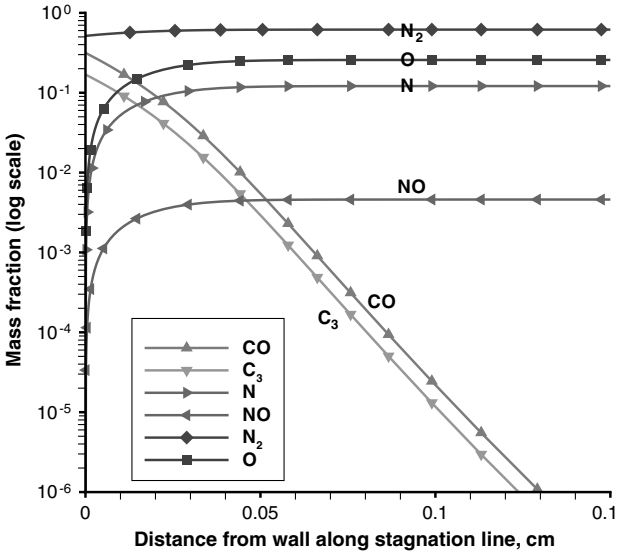

Fig. 12 Chemical species distributions along the stagnation streamline.

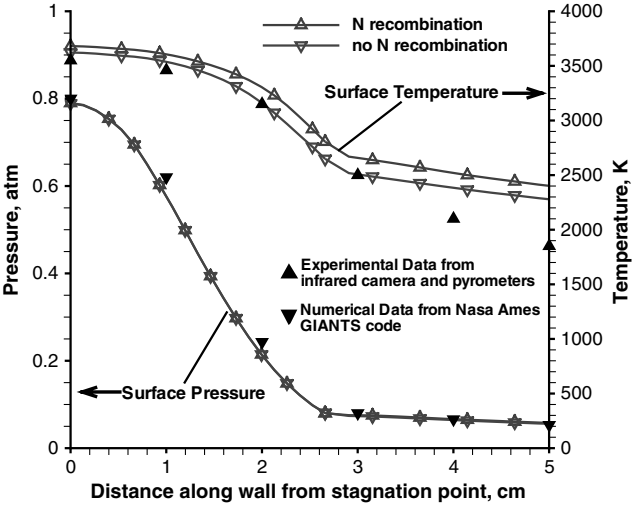

Fig. 14 Measured (from [10]) and predicted surface temperature and pressure distributions along the surface with and without atomic nitrogen recombination.

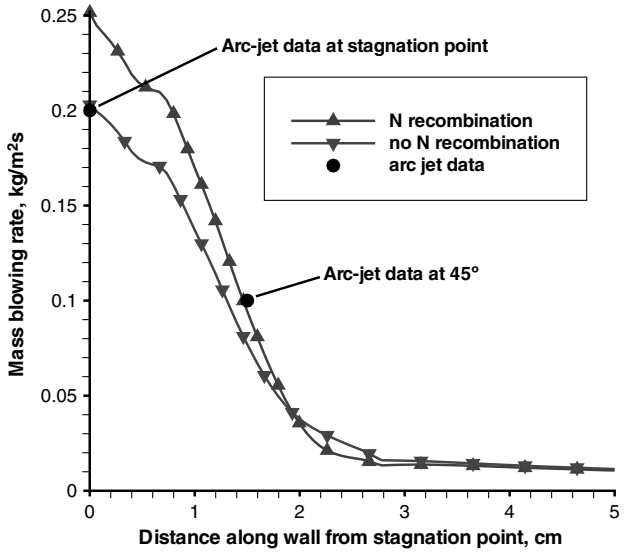

Fig. 15 Measured (from [10]) and predicted mass blowing rate distributions along the surface with and without atomic nitrogen recombination.

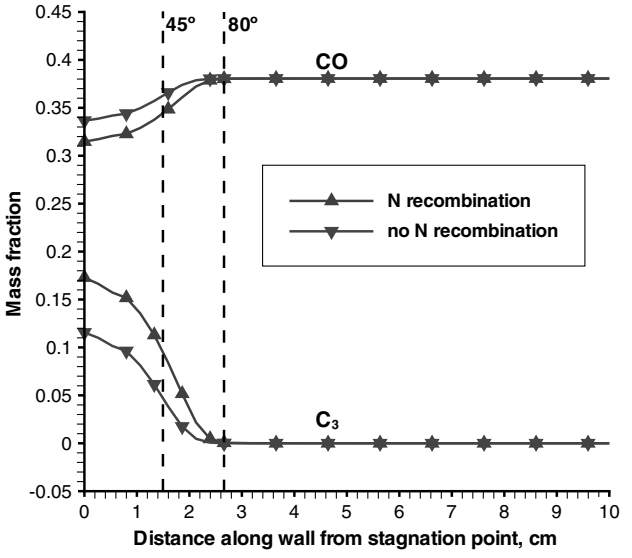

Fig. 16 Predicted CO and C3 mass fraction distribution along the surface with and without atomic nitrogen recombination.

stagnation point causes a strong reduction (20%) in the ablation rate. The importance of a coupled ablation analysis without the use of approximations has been assessed in [6] for diffusion-limited oxidation. In such a regime, the surface temperature has a weak influence on the ablation mass flux. In the present condition, in which oxidation/sublimation transition is reached, the surface mass and energy balances are strongly coupled and hence a coupled ablation-flowfield approach is deemed even more necessary.

V. Conclusions

A model based on a full Navier–Stokes approach has been used to examine thermochemical ablation of graphite in hypersonic reentry environments. The two regions, gas and solid, are fully coupled at the surface by appropriate energy and mass balances, allowing the surface conditions to be solved as part of the overall solution. The surface thermochemistry model is based on heterogeneous chemical equilibrium and can account for both surface oxidation and sublimation. Even if a surface nonequilibrium treatment is a more general approach, the present model permits a simplification of the problem formulation with reasonable accuracy for many practical conditions. Indeed, the predicted surface recession rates show a good agreement with the available experimental data. A laminar supersonic flow over a spherically blunted cone has been simulated and numerical solutions were successfully obtained and compared with measured data obtained from arc jet tests. The calculations slightly overpredict the surface temperature in the spherical region (5% maximum) and the error reaches its maximum (30%) in the conical region, where surface temperature drops below 2500 K (which is a limiting value for equilibrium calculations). The presented equilibrium model overpredicts the graphite mass blowing rate by about 25% at the stagnation point and underpredicts it by less than 5% at 45 deg from the stagnation point. Surface equilibrium computation dictates a complete recombination of atomic nitrogen at the surface for the actual pressure and temperature conditions. According to experimental observation, which has shown nitrogen atom recombination not to occur to any measurable extent, a new simulation of the test case has been recomputed by freezing this recombination reaction. The result is a noticeably improvement of the agreement with experimental data in the stagnation point: the error is reduced from 25 to 1.5%. The agreement with the experimentally measured surface temperature is also improved with the maximum error in the stagnation-point region decreasing from 5 to 2% and in the conical region from 30 to 23%. The obtained results can be considered as very interesting, because both surface temperature and surface blowing rate have been predicted reasonably well without the need of imposing the experimental surface temperature distribution. Indeed no assumptions have been made on the ablation rate or on wall temperature distributions and both have been calculated from the ablation surface balances integrated in the flow solver.

Acknowledgments

This study was performed in the frame of the TRP (Technology Research Programme) on Multiphysics Modeling of Near Surface Phenomena, contract no. 19168/05/NL/IA with the ESA European Space Research and Technology Centre, under the supervision of M. Onofri.

References

[1] Milos, F. S., and Rasky, D. J., "Review of Numerical Procedures for Computational Surface Thermochemistry," *Journal of Thermophysics and Heat Transfer*, Vol. 8, No. 1, 1994, pp. 24–34. doi:10.2514/3.497

[2] Kuntz, D. W., Hassan, B., and Potter, D. L., "Predictions of Ablating Hypersonic Vehicles Using an Iterative Coupled Fluid/Thermal Approach," *Journal of Thermophysics and Heat Transfer*, Vol. 15, No. 2, 2001, pp. 129–139. doi:10.2514/2.6594

[3] Chen, Y. K., and Milos, F. S., "Two-Dimensional Implicit Thermal Response and Ablation Program for Charring Materials," *Journal of Spacecraft and Rockets*, Vol. 38, No. 4, 2001, pp. 473–481. doi:10.2514/2.3724

[4] Bianchi, D., Nasuti, F., and Martelli, E., "Coupled Analysis of Flow and Surface Ablation in Carbon-Carbon Rocket Nozzles," *Journal of Spacecraft and Rockets*, Vol. 46, No. 3, 2009, pp. 492–500. doi:10.2514/1.40197

[5] Bianchi, D., Nasuti, F., Martelli, E., and Onofri, M., "A Numerical Approach for High-Temperature Flows over Ablating Surfaces," AIAA Paper 2007-4537, 2007.

[6] Johnston, C. O., Gnoffo, P. A., and Mazaheri, A., "A Study of Ablation-Flowfield Coupling Relevant to the Orion Heatshield," AIAA Paper 2009-4318, 2009.

[7] Havstad, M. A., and Ferencz, R. M., "Comparison of Surface Chemical Kinetic Models for Ablative Reentry of Graphite," *Journal of Thermophysics and Heat Transfer*, Vol. 16, No. 4, 2002, pp. 508–515. doi:10.2514/2.6725

[8] Olynick, D., Chen, Y. K., and Tauber, M. E., "Aerothermodynamics of the Stardust Sample Return Capsule," *Journal of Spacecraft and Rockets*, Vol. 36, No. 3, 1999, pp. 442–462. doi:10.2514/2.3466

[9] Chen, Y. K., Milos, F. S., Reda, D. C., and Stewart, D. A., "Graphite Ablation and Thermal Response Simulation under Arc-Jet Flow

Conditions," AIAA Paper 03-4042, 2003.
[10] Chen, Y. K., and Milos, F. S., "Navier–Stokes Solutions with Finite Rate Ablation for Planetary Mission Earth Reentries," *Journal of Spacecraft and Rockets*, Vol. 42, No. 6, 2005, pp. 961–970. doi:10.2514/1.12248
[11] Moyer, C. B., and Rindal, R. A., "An Analysis of the Chemically Reacting Boundary Layer and Charring Ablator. Part II: Finite Difference Solutions for the In-Depth Response of Charring Materials Considering Surface Chemical and Energy Balances," NASA CR 1061, 1968.
[12] Quan, V., "Quasi-Steady Solution for Ablation-Erosion Heat Transfer," *Journal of Spacecraft and Rockets*, Vol. 7, No. 3, 1970, pp. 355–357. doi:10.2514/3.29938
[13] Bianchi, D., "Modeling of Ablation Phenomena in Space Applications," Ph.D. Dissertation, Università Degli Studi di Roma "La Sapienza," Rome, Jan. 2008.
[14] Bhutta, B. A., and Lewis, C. H., "Low-to-High Altitude Predictions of Three-Dimensional Ablative Hypersonic Flowfields," *Journal of Spacecraft and Rockets*, Vol. 30, No. 4, 1993, pp. 395–403. doi:10.2514/3.25544
[15] Gupta, R. N., "Aerothermodynamic Analysis of Stardust Sample Return Capsule with Coupled Radiation and Ablation," *Journal of Spacecraft and Rockets*, Vol. 37, No. 4, 2000, pp. 507–514. doi:10.2514/2.3592
[16] Zhluktov, S. V., and Abe, T., "Viscous Shock-Layer Simulation of Airflow past Ablating Blunt Body with Carbon Surface," *Journal of Thermophysics and Heat Transfer*, Vol. 13, No. 1, 1999, pp. 50–59. doi:10.2514/2.6400
[17] Gordon, S., and McBride, B. J., "Computer Program for Calculation of Complex Chemical Equilibrium Compositions and Applications," NASA RP 1311, 1994.
[18] Martelli, E., "Studio Della Fluidodinamica Interna di Ugelli Propulsivi di Tipo Dual Bell," Ph.D. Dissertation, Università Degli Studi di Roma "La Sapienza," Rome, Jan. 2006 (in Italian).
[19] Nasuti, F., and Onofri, M., "Analysis of Unsteady Supersonic Viscous Flows by a Shock Fitting Technique," *AIAA Journal*, Vol. 34, No. 7, 1996, pp. 1428–1434. doi:10.2514/3.13249
[20] Moretti, G., "A Technique for Integrating Two-Dimensional Euler Equations," *Computers and Fluids*, Vol. 15, No. 1, 1987, pp. 59–75. doi:10.1016/0045-7930(87)90005-3
[21] Milos, F. S., and Chen, Y. K., "Ablation and Thermal Response Property Model Validation for Phenolic Impregnated Carbon Ablator," 47th AIAA Aerospace Sciences Meeting, Orlando, FL, AIAA Paper 2009-262, Jan. 2009.
[22] Stewart, D. A., "Surface Catalysis and Characterization of Proposed Candidate TPS for Access-to-Space Vehicles," NASA TM 112206, 1997.
[23] Park, C., "Stagnation-Point Radiation for Apollo 4," *Journal of Thermophysics and Heat Transfer*, Vol. 18, No. 3, 2004, pp. 349–357. doi:10.2514/1.6527
[24] Park, C., "Calculations of Stagnation-Point Heating Rates Associated with Stardust Vehicle," *Journal of Spacecraft and Rockets*, Vol. 44, No. 1, 2007, pp. 24–32. doi:10.2514/1.15745

T. Lin
Associate Editor